TRANSACTIONS ON ELECTROMAGNETIC SPECTRUM

# Development of a MATLAB Tool for Antenna Diagnostics Using Amplitude-only Field Measurement and Source Reconstruction Method

**Asha Karmur[1], Rizwan H. Alad[1*], Purvang Dalal[1], Hetvi Makwana[1]**

[1]Department of Electronics& Communication, Faculty of Technology, Dharmsinh Desai University, Nadiad, India
Email: 22ecubg109@ddu.ac.in, rizwan_alad.ec@ddu.ac.in, pur_dalal.ec@ddu.ac.in, 22ecuog119@ddu.ac.in

*** Corresponding author's e-mail address:** rizwan_alad.ec@ddu.ac.in

**Received:** 23 October 2025
**Revised:** 25 December 2025
**Accepted:** 9 January 2026

**Research Article**
**Vol. 5 / No. 1 / 2026**
**Doi: 10.65819/tes.2026.v5i1.63**

**Abstract:** A graphical user interface (GUI) tool for non-invasive antenna diagnostics using amplitude-only field measurements and the Source Reconstruction Method (SRM) was developed in MATLAB. The tool allows users to import or to simulate measurement data and select the measurement surface (planar, cylindrical, spherical, or poly-planar). Various algorithmic options are provided, including phase-retrieval approaches such as the Gerchberg–Saxton method, Hybrid Input–Output (HIO), and sparse regularization, as well as forward solvers based on the Fast Multipole Method (FMM) and the Method of Moments (MoM). The reconstructed equivalent current distribution is used to compute the corresponding far-field radiation characteristics, including 2D radiation patterns and beam direction, which are visualized through built-in reporting tools. Even without phase information, the SRM implementation can recover element excitations and surface currents with high accuracy by combining regularization techniques with iterative inversion to mitigate the ill-posed nature of the problem. Simulation results on the reconstruction of electromagnetic fields on canonical antenna structures have revealed that the proposed method is able to reconstruct the electromagnetic fields with a reconstruction error of less than 10%, on average, when the SNR is 20 dB. The proposed MATLAB tool is a cost-effective platform for testing and fault diagnosis of the antenna. It is applicable to the field of satellite communication systems, phased array antennas, and radar.

**Keywords:** Field measurement, Source reconstruction method, Phaseless inverse problem, Antenna array, MATLAB-based GUI

**Cite this paper as:** Karmur A., Alad RH., Dalal P., Makwana H. Development of a MATLAB Tool for Antenna Diagnostics Using Amplitude-only Field Measurement and Source Reconstruction Method. Transactions on Electromagnetic Spectrum. 2026; 5(2): 12-24, Doi: 10.65819/tes.2026.v5i1.63

## 1. INTRODUCTION

Diagnostics in antenna technology has witnessed major advancements in recent decades, starting from microwave holographic methods and reflector surface error analysis in the 1960s and 1970s, and moving towards near-field-to-far-field transformation, which has become an accepted method in antenna characterization in the 1980s and 1990s [1, 2]. The subsequent development of the Source Reconstruction

Method (SRM) in the 2000s led to the reconstruction of equivalent current distributions based on the principles of electromagnetic fields, thus creating a significant role for SRM in antenna diagnosis and verification [3]. Recent research has been carried out on phaseless inversion and compressed sensing methods for effective and cost-saving antenna testing. Antenna array structures are of great importance for various modern communication, radar, and space technologies owing to their potential to regulate beam steering and radiation patterns by appropriately exciting the antenna array elements. By appropriately adjusting the excitation magnitude of the antenna array elements, it is possible to concentrate the radiated signal in a particular direction while suppressing undesired interferences in other directions [4]. In such scenarios, it is important to visualize the radiation pattern in three-dimensional format for various antenna-related activities like diagnosis, assessment, and maintenance. In conventional antenna analysis, direct or forward methods based on electromagnetic techniques, such as the Method of Moments, Finite Element Method, and Boundary Element Method, are commonly used, which give precise results when the antenna geometry and excitation are known [4-6]. However, these methods are found to be ineffective for post-fabrication diagnosis and fault detection when the internal antenna parameters are unknown. In order to overcome the above problems, several inverse methods have been proposed, and among them, the Source Reconstruction Method is found to be the most effective method [3, 7, 8]. The SRM is used for reconstructing equivalent electric and magnetic currents from the available measurements of the electromagnetic field. This allows for the calculation of the far-field radiation patterns, fault localization, and performance assessment. In traditional SRM, both amplitude and phase information are required. This is often obtained by using near-field measurements and near-field-to-far-field transformations, NF-FF [2, 7]. However, phase information is often difficult and expensive to measure in real-world applications, such as satellite antenna testing and phased arrays [9]. This challenge has inspired the development of phaseless SRM methods, in which only the magnitude of the electromagnetic fields is used in the measurement process [10]. While using only the magnitude of the electromagnetic fields greatly simplifies the system in terms of complexity and cost, it poses an ill-posed problem in which multiple source distributions may have the same magnitude of the electromagnetic fields [10]. In order to deal with this problem, various stabilization techniques like Tikhonov regularization, sparsity constraints, as well as various phase retrieval algorithms like Gerchberg-Saxton, Hybrid Input-Output (HIO), convex optimization, etc., have been extensively studied [6, 11-14]. In addition to this, for electrically large antennas as well as dense grid structures, the computational cost of SRM is a problem that needs to be dealt with. The use of acceleration techniques like Fast Multipole Method (FMM) has reduced the computational cost from O(N2) to O(N log N) or even O(N). In addition to this, various scanning geometries like poly-planar near-field scanning are also being employed when canonical geometries are not feasible [1, 15, 16]. Nonetheless, the challenge of integrating phase-less SRM, regularization, phase retrieval, and computational speedup into a single and user-friendly package persists. In order to bridge the existing gap, the current work proposes a graphical user interface tool for non-invasive antenna diagnostics based on measurements of antenna fields' magnitudes and the Source Reconstruction Method. The proposed tool is based on the integration of phase retrieval techniques, regularized SRM, and computational speedup for original source reconstruction and computation of 2D/3D radiation patterns, ray directions, and nulls. The proposed tool is a cost-effective solution for antenna verification of satellites, phased array antennas, and educational purposes, as it removes the need for direct phase measurement while providing a user-friendly interface.

## 2. PROBLEM FORMULATION

In antenna array diagnostics, the final aim is to diagnose the state of an antenna array without any disassembly and without making use of any complicated measurement systems. In conventional methods, it is necessary to have both the magnitude and phase information of the radiated fields. This can be achieved through either near-field or far-field measurement systems. It has been observed that phase information is not only expensive, but it can also lead to incorrect results due to environmental conditions. In some cases, only magnitude information can be made use of, as in satellites and ground-based antenna arrays, due to inaccessibility [17-19]. The radiated electromagnetic field is described by Maxwell's equations, which describe the interaction between electric and magnetic fields. The relation between the observed field and source distribution is expressed in [12, 20]:

$$E(r) = \int_S \mathrm{G}(\mathrm{r}, \mathrm{r}')\, J(r')\, dS' \tag{1}$$

Where:

 

$E(r)$: Electric field at observation.
$J(r')$: Equivalent current distribution.
$G(r, r')$ : Green's function describing the electromagnetic interaction between the source and observation points [12, 21]:

Since phase information is missing in the data, the reconstruction becomes ill-posed. In fact, several current distributions may produce the same magnitude [3]. In order to tackle this challenge, several sophisticated techniques and methods are applied.

### 2.1 Tikhonov Regularization

The inverse reconstruction process is very sensitive to measurement noise, where small noise can cause large errors in the solution. Tikhonov regularization is a method of stabilizing the inverse problem by adding a term:

$$\frac{min}{J} \; |||E_{meas}| - |E_{meas}(J)|||_2^2 + \; \lambda R(J) \tag{2}$$

Here, λ controls the smoothness of the solution.

Where:
$R(J)$: Regularization functional (e.g., Tikhonov $L_2$ norm [6] for smoothness or$L_1$norm [31] for sparsity),
$\lambda$ : A weighting factor controlling the trade-off between fidelity to measurements and stability of the solution. This ensures a stable and smooth current distribution but may reduce resolution.
|Emeas|: Measured magnitude of the electric field
|Emeas(J)|: Magnitude of the electric field predicted by the model for a given current distribution
J: Equivalent current distribution on the reconstruction surface

### 2.2 Conjugate Gradient Method (CGM)

The Conjugate Gradient Method (CGM), as an iterative optimization technique, is employed to solve large-scale inverse problems. Instead of directly computing the inverse of the matrices, which is computationally intensive, the CGM method uses an iterative approach that improves the solution by steps along the conjugate directions. This method is faster than the gradient descent method. In the SRM method, the CGM method is employed to efficiently calculate the source. As the phase is not directly accessible, it needs to be retrieved using various algorithms. The Gerchberg–Saxton (GS) algorithm is an iterative algorithm that switches between the spatial and Fourier domains while incorporating the given amplitude constraints. The Hybrid Input-Output (HIO) algorithm is an advanced version of the iterative algorithm that resolves the stagnation problem. Reweighted Amplitude Flow (RAF) employs optimization with adaptive weights to robustly recover phases. These methods provide approximate phase information, enabling SRM to operate using magnitude-only measurements.

### 2.3 Fast Multipole Method (FMM)

For large arrays, the direct computation of the Green function integrals would take O ($N^2$) operations. However, the Fast Multipole Method (FMM) can reduce the computational complexity of SRM to O (N log N) operations by grouping the sources in clusters and using multipole expansions. SRM becomes computationally feasible for arrays with thousands of elements, as in satellite and radar applications.

It incorporates SRM with phase retrieval constraints and updates the current distribution based on magnitude matching and smoothness. This improves the robustness of the technique under noisy and incomplete data conditions. Phase information cannot be found in magnitude-only measurements because these only give the amplitude of the field |E(r)|. Since phase information cannot be found in magnitude-only measurements, multiple current distributions can produce the same magnitude of the field only compliances, which only give the field's magnitude |E(r)|. Since the absence of phase information allows multiple current distributions to reproduce identical field bulks, the inverse reconstruction lacks oneness [3]. For stabilizing and solving the inverse problem, advanced techniques like regularization and optimization have to be employed. Phase

 

retrieval algorithms, including the Gerchberg-Saxton algorithm [19], Hybrid Input-Output (HIO), and Reweighted Amplitude Flow (RAF), are utilized in the reconstruction algorithm. After applying the Near-Field to Far-Field (NF-FF) transformation, the Source Reconstruction Method is applied for source reconstruction, making use of the retrieved phases [3, 18]. For solving inverse problems, conventional Source Reconstruction Methods require both magnitude and phase information. Even if both pieces of information are available, solving methods like Tikhonov regularization, iterative phase recovery, and the Conjugate Gradient Method can be computationally expensive and sensitive to noise. Moreover, SRM itself is sensitive to noise, making it difficult to apply complex regularization methods and iterative algorithms. Yet, SRM is significant in both near-field and far-field diagnostics. This study seeks to investigate some strategies that can improve SRM's efficacy, particularly in cases where only magnitude information is available [12, 18, 19].

In the context of the present work, the problem is further specified for array-specific diagnostics, in which the array parameters (number of elements N, element spacing d, and operating frequency) are known. The radiating element type is also known and is described by analytical equations. Only the far-field magnitude over a set of angular samples is available. Due to the large size of the measurement data sets, often containing thousands of data points, the Fast Multipole Method is employed to reduce the computational complexity from $O(N^2)$ to $O(N \log N)$ with no accuracy compromise [9, 22, 23]. The main steps of the FMM are the hierarchical spatial decomposition of the problem, the multipole expansions, the direct calculation for near-field interactions, and the multipole-to-local translation and aggregation [24].

The proposed framework can be utilized in solving the problem related to antenna array diagnostics, particularly in cases where only the magnitude information in the radiation pattern is available. This includes the reconstruction of the complex excitation currents applied to individual elements in the array, determining the direction of arrival (DoA) of the main beam, and identifying null positions in the radiation pattern. This can be accomplished through an appropriate measurement geometry, phase recovery methods, solving the SRM inverse problem, and comparing the reconstructed electric fields with those from an analytical or simulated model.

### 2.4 SRM Methodology

The Source Reconstruction Method is a physics-based inverse method used in the diagnosis of antennas through the reconstruction of the original source distributions from the known electromagnetic fields. In the proposed method, SRM is utilized with only magnitude measurement data and incorporated in a MATLAB-based graphical user interface (GUI) for the non-invasive diagnosis of antennas [3, 7, 8]. The methodology first involves obtaining electromagnetic field data over a specified measurement surface, which can be planar, spherical, curved, or even poly-planar, depending on the nature of measurement. In the phase-less approach, only the electric field's amplitude is measured, thereby reducing the instrumentation and cost of measurement. These field data samples form the input to the reconstruction process [15, 21, 22]. Using the electromagnetic equivalence principle, the measured fields are expressed as a function of the original electric or magnetic surface currents distributed on the assumed reconstruction surface that covers the antenna under test. This gives rise to an inverse problem where the unknown source currents are related to the measured fields using Green's functions. Since the measurement provides only the magnitude of the field, the inverse problem that arises is ill-posed and non-unique [12, 20, 23]. To maintain stability in the inversion process and eliminate the impact of noise, regularization techniques are often incorporated into the SRM. For instance, Tikhonov regularization and sparsity constraints are often employed to enforce smoothness or simplicity in the reconstructed current distribution. Additionally, the Gerchberg–Saxton algorithm and the Hybrid Input–Output (HIO) method are often incorporated to retrieve the missing phases from the available magnitude data [19]. These techniques are often effective in the reconstruction of the complex-valued original sources [3, 18].

The inverse problem can be solved numerically using iterative optimization techniques, where the Conjugate Gradient Method is employed to avoid the inversion of the matrix and efficiently handle large-scale problems. For electrically large antennas and dense measurement grid cases, the Fast Multipole Method is employed to speed up the calculation of the interactions of the Green's function, reducing the computational complexity of the algorithm [1, 6, 15, 16]. The reconstructed source distribution can now be employed in the computation of

 

the far-field characteristics of the antenna. Some of the important characteristics of the antenna, such as the radiation pattern, beam axes, nulls, and excitation coefficients, can be extracted from the reconstructed fields. These results can now be visualized using various plots in both 2D and 3D formats through the GUI of the program [3, 7, 13].

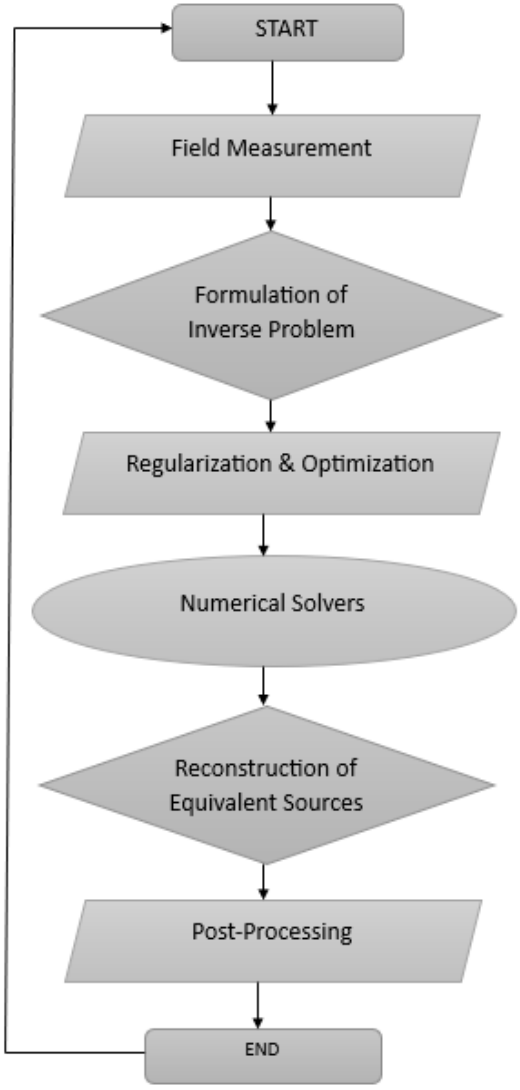


**Figure 1:** Overview of the proposed antenna array workflow using magnitude-only measurements and the SRM.

The proposed tool would be able to efficiently and accurately diagnose antennas using only magnitude-based SRM measurements, which would be beneficial in various applications including phased array verification, satellite antenna testing, and educational purposes.

## 3. NUMERICAL RESULTS AND DISCUSSIONS

The developed MATLAB-based GUI was successful in generating the 2D normalized radiation patterns of various types of antennas, including helical and dipole antennas, using parameters specified by the user, e.g., the number of elements in the antenna ($n$), spacing between the elements ($d$), and the frequency of operation ($f$). It was also successful in generating the 2D principal-planes cut (φ = 90°) of the antennas using the 2D radiation pattern, which helped in accurately determining the DoA with null locations in agreement with theoretical results.

All simulations employed a uniform linear array (ULA) of equal elements positioned along the x-axis with element locations specified by $m$=1, 2,…,$N$ and a specified element spacing $d$ in terms of wavelengths. The

 

frequency of operation was $f$=1 GHz with a corresponding wavelength of 0.3 m and a wave number of $k$=20 rad/m. The array factor used in the GUI is,

$$AF\ (\theta, \phi) = \ \sum_{m}^{n-1} J(\theta)\, e^{-jkmd\cos\theta} \tag{3}$$

Where:

J(θ) : Single-element pattern (dipole: $|\sin\theta|$; spiral: broadband empirical shape used in the GUI)
k : Free space wave number
$\theta$ : Elevation angle measured from the array axis
$\phi$ : Azimuth angle
m: Element index
d : Inter-element spacing

The 2D elevation cuts were obtained at φ = 90° and the azimuth cuts at θ = 90°. The radiation patterns of the antenna arrays were analyzed by varying the number of elements (N) while keeping the inter-element spacing (d) constant, and by varying d while keeping N constant. The normalized radiation pattern shown in Figure 2 corresponds to the dipole antenna array. Similar simulations were also performed for helical and circular antenna arrays under the same conditions (N=8, d=0.5λ), which exhibited comparable radiation characteristics. Therefore, only the dipole array pattern is presented for brevity.

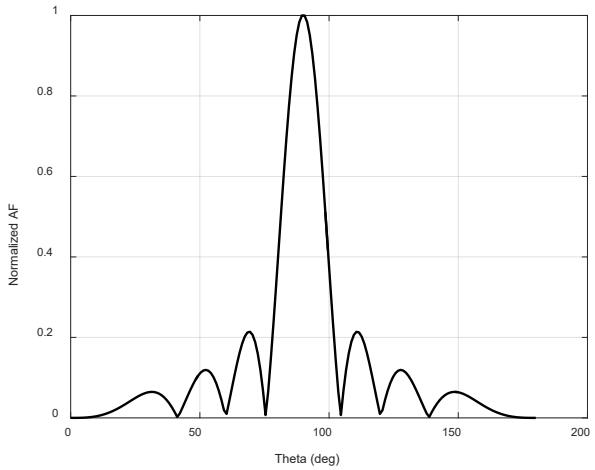


**Figure 2:** Normalized radiation patterns of dipole antenna arrays with N = 8 elements and an inter-element spacing of d=0.5λ, highlighting the main-lobe width and side-lobe characteristics for comparative analysis.

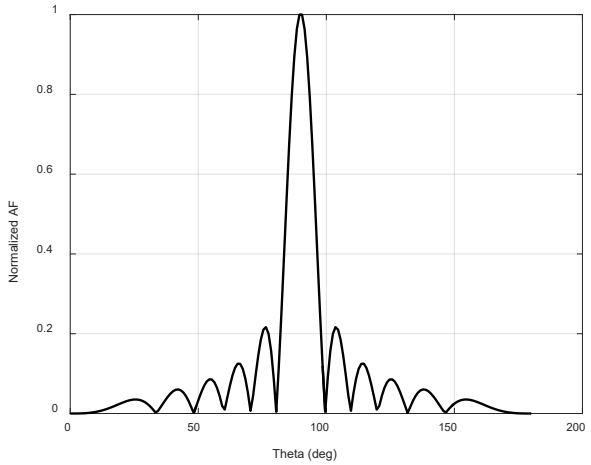


**Figure 3:** Normalized radiation patterns of dipole antenna arrays with N = 12 elements and an inter-element spacing of d=0.5λ, showing beam narrowing and improved directivity with an increased number of elements, enabling the evaluation of array performance.

 

As shown in Figure 3, increasing the number of array elements from N = 8 to N = 12 while maintaining the spacing d = 0.5λ results in a narrower main lobe and improved directivity. The same simulation was performed for helical and circular antenna arrays, and a similar improvement in directivity was observed. This confirms that increasing the number of elements effectively increases the array aperture, thereby concentrating the radiated energy in the desired direction.

When the value of $N$ is increased, keeping the inter-element spacing fixed, the main lobe becomes narrower, and the directivity is improved. This is because, by increasing the number of elements, the effective aperture is larger, thus directing the beam in the required direction. Although side lobes are also present, their relative amplitude is reduced with an increase in the number of elements.

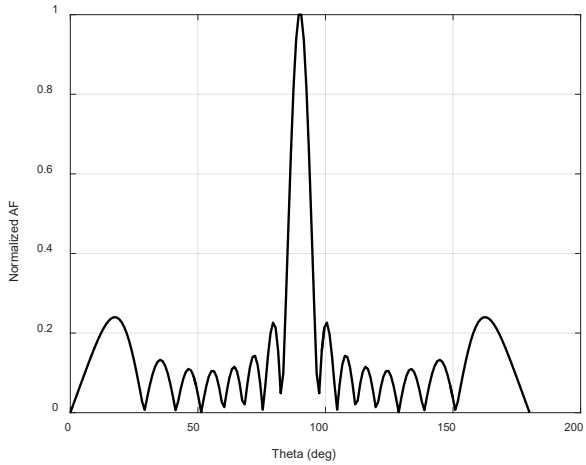


**Figure 4:** Radiation patterns of dipole antenna arrays (N=8, d=1λ), showing the initial development of side lobes as the inter-element spacing increases.

Figure 4 illustrates the radiation pattern of the dipole array when the element spacing is increased to d = 1λ. Under the same configuration, the helical and circular arrays also exhibit similar radiation behavior, where the side-lobe levels begin to increase as the spacing between elements grows. This demonstrates the sensitivity of antenna array radiation patterns to variations in element spacing.

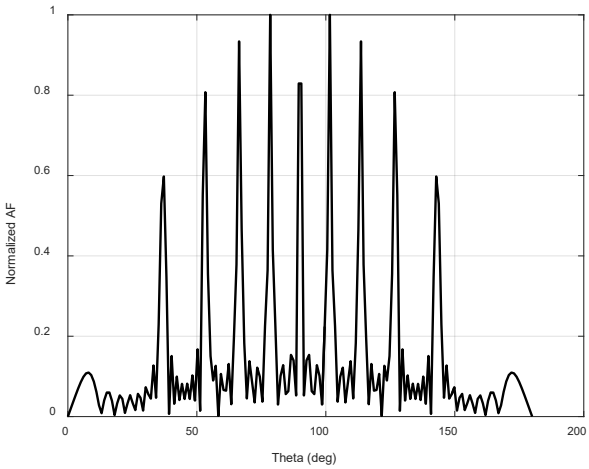


**Figure 5:** Radiation patterns of dipole antenna arrays with N=8 elements and d=2λ, illustrating grating lobe formation caused by excessive element spacing.

As illustrated in Figure 5, when the spacing between array elements is increased to d = 2λ, strong grating lobes appear in the radiation pattern. Similar results were obtained for helical and circular antenna arrays, indicating that excessive spacing leads to the formation of additional unwanted lobes regardless of the antenna element type. These grating lobes degrade the radiation performance and reduce the effectiveness of the antenna array.

On the other hand, if the spacing between elements, denoted as $d$, is increased, the array's behavior is quite different. For $d \leq \lambda$, the radiation characteristics are good, with a single lobe and manageable side lobes.

 

However, for $d > \lambda$, for instance, when $d = 2\lambda$, the array's radiation characteristics are impaired by the appearance of additional lobes, referred to as grating lobes, which are maxima of the array's radiation pattern except for the main beam. Thus, in brief, an increase in the number of elements $N$ improves directivity without the presence of grating lobes. On the contrary, an increase in the distance between the array elements beyond the wavelength $\lambda$ gives rise to grating lobes that spoil the radiation pattern.

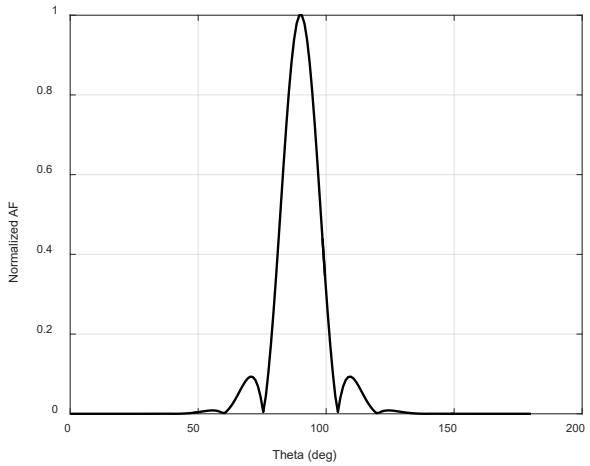


**Figure 6:** Normalized radiation pattern of the linear antenna array (N=8 and d=0.5λ), showing the characteristics of the main lobe and side-lobe levels.

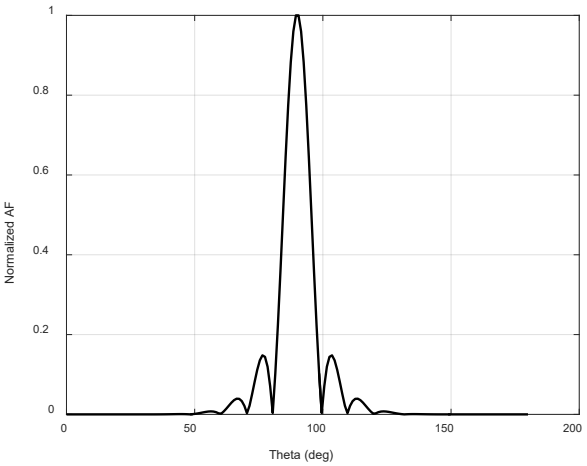


**Figure 7:** Radiation pattern of a 12-element linear antenna array with an inter-element spacing of d=0.5λ, showing improved directivity and reduced beam width, which helps suppress side-lobes and minimize interference.

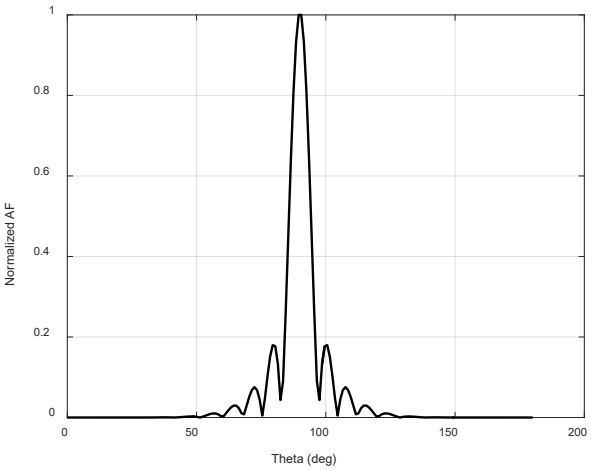


**Figure 8:** Normalized radiation pattern of the linear antenna array (N=8) in the φ=90° plane, illustrating the pattern shape and main-lobe characteristics used for direction of arrival (DoA) estimation and null position analysis.

 

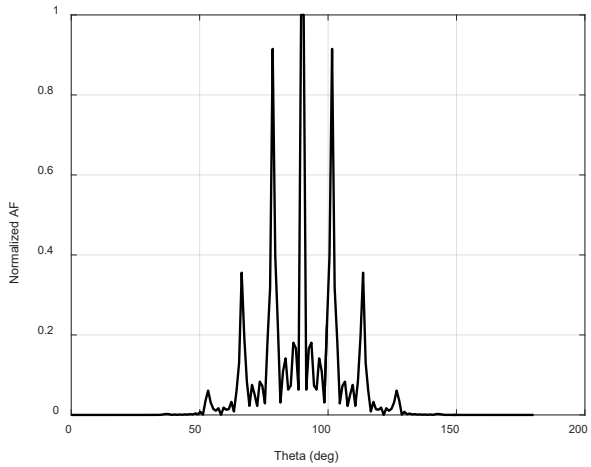


**Figure 9:** Radiation pattern of the linear antenna array (N=8) with a large inter-element spacing (d=2λ), illustrating the emergence of grating lobes caused by excessive element spacing and the resulting degradation in array performance.

From the results below, it can be observed that for a given number of elements $N$=8, the spacing between elements $d$ has a significant impact on the beam width and side lobe characteristics of the radiation pattern. At a smaller spacing between elements given by $d$=0.5$\lambda$, the main lobe is relatively broad and side lobes are weaker and less defined. As a result, a uniform radiation pattern is obtained. When the spacing between elements is increased to $d$=1$\lambda$ and further to $d$=2$\lambda$, the main lobe becomes narrower. Hence, a high directivity is obtained from the array. At increased spacing between elements, multiple grating lobes can be observed as sharp peaks in the radiation pattern. This trade-off suggests that not only does increasing the spacing of the element improve the resolution and sharpness of the beam but also results in the creation of undesired grating lobes. Hence, the selection of an optimal spacing between the array elements is of prime importance to achieve an optimal balance between minimizing the beam width and minimizing the grating lobes.

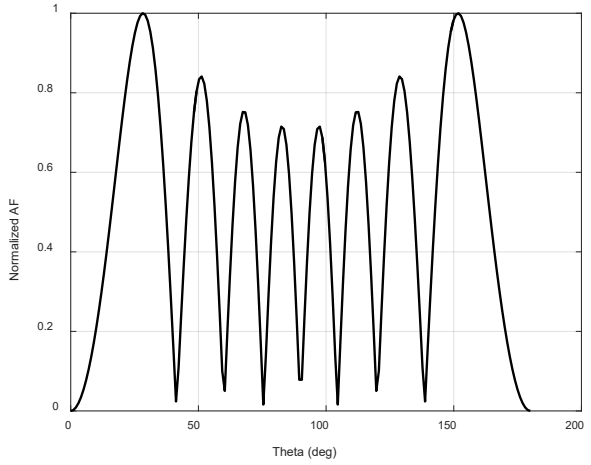


**Figure 10:** Radiation pattern of the monopole antenna array with N=8 and d = 0.5λ, indicating a good main lobe with minimum grating lobes for better diagnostic applications.

From the results, the design consideration for the monopole array can be clearly deduced from the selected values for the spacing $d$ and the number of elements $N$. From the results, it is clear that as the spacing between the elements increases, i.e., for $d$=2$\lambda$, the main lobe becomes narrower, but the grating lobes are strong, which makes the antenna less suitable for use in diagnostics. However, when the spacing between the elements is $d$=0.5$\lambda$, the grating lobes are eliminated, the main lobe becomes wider, and the side lobes are lower. Moreover, as the number of elements increases for the spacing $d$=0.5$\lambda$, the main lobe becomes narrower, the directivity increases, but the number of side lobes increases.

 

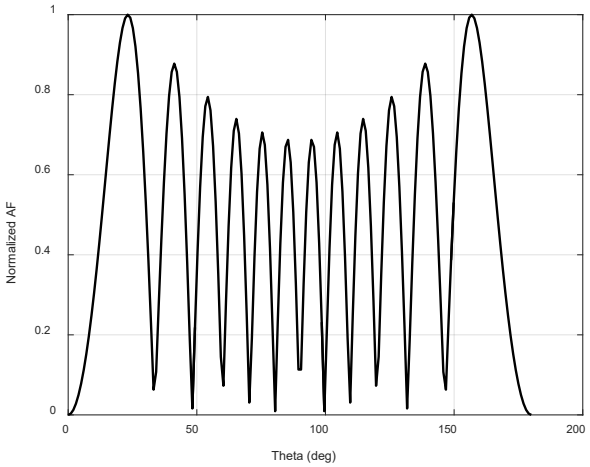


**Figure 11:** Radiation pattern of the monopole antenna array with N=12 and d=0.5λ, illustrating a narrower beam and enhanced directivity resulting from side-lobe reduction, which aids in evaluating array performance.

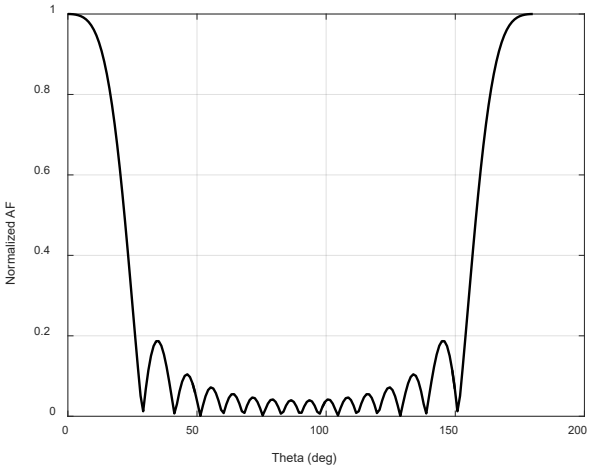


**Figure 12:** Radiation pattern of the monopole antenna array with N=8 and d=1λ, showing changes in side-lobe levels and beam width as the inter-element spacing approaches the onset of grating lobes.

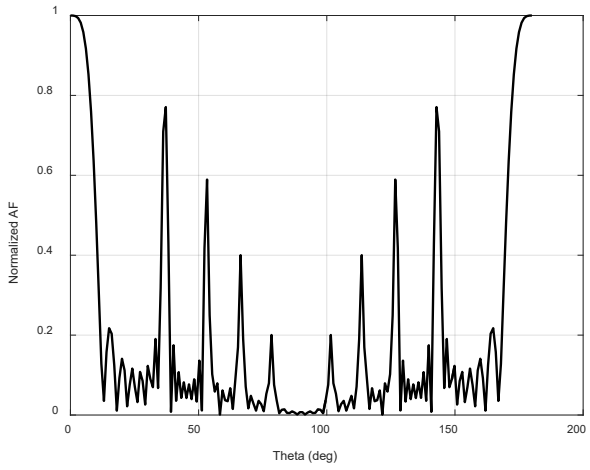


**Figure 13:** Radiation pattern of the monopole antenna array with N=8 and d = 2λ, illustrating pronounced grating lobes resulting from overly large inter-element spacing, which degrades array performance.

It has been observed from the simulated radiation patterns that the spacing between the elements and the number of elements in the antenna array are quite significant in improving the performance of the antenna array. When the spacing between the elements is increased by choosing a larger value for the spacing parameter ($d$), for example, $d=2\lambda$, the main lobe is reduced. However, strong grating lobes are present in the radiation

 

pattern, which may reduce the performance of the antenna array. On the other hand, when the spacing between the elements is optimal, that is, $d$=0.5$\lambda$ the grating lobes are absent in the radiation pattern. The radiation pattern is clear and stable in this case. When the number of elements is increased for this optimal value of ($d$), the directivity of the antenna array improves along with a narrower main lobe. In this case, the number of side lobes is increased, which may reduce the effectiveness of the antenna. Hence, a compromise may be achieved by choosing a half-wavelength spacing between the elements along with a larger number of elements.

It allows the export of all calculated results (radiation pattern, locations of DoA/nulls, excitation amplitudes/phases) to Excel format. It allows saving the visualizations to PNG format. The GUI provides intuitive control over the parameters, allowing real-time parameter adjustments. This tool is useful for iterative design processes, educational purposes, and comparison of antennas.

In this study, a MATLAB-based GUI framework for antenna array simulation, radiation pattern visualization, and source reconstruction was successfully developed, where antenna array simulation, radiation pattern visualization, and source reconstruction are combined in a unified platform, where users can input parameters such as the number of elements, spacing, frequency, and antenna type, and instantly visualize their effects on two-dimensional radiation characteristics. Unlike other conventional methods, which are costly as they demand phase measurement, the implemented Source Reconstruction Method, as discussed in this study, can estimate source excitation amplitude and phase using amplitude (magnitude) far-field data, making it a cost-effective and feasible approach for antenna array simulation and source reconstruction. The GUI provides a clear visualization of important radiation parameters, such as main lobe, nulls, beam width, and Direction of Arrival (DoA). It is also capable of exporting results in Excel and PNG formats for verification purposes. This study combines theoretical modeling, numerical reconstruction, and visualization in a comprehensive framework, which can be useful for supporting further research, educational purposes, and validation of phased array antennas in real-world applications, such as those related to ISRO.

## 4. QUANTITATIVE ERROR ANALYSIS AND ROBUSTNESS EVALUATION

In order to further support the qualitative agreement that is evident from the plots of the radiation patterns, a systematic quantitative error analysis has been performed to assess the accuracy and robustness of the proposed amplitude-only SRM framework. The accuracy of the reconstructed far-field patterns has been quantitatively compared with the theoretical or analytically derived patterns.

The relative reconstruction error is defined as

$$\varepsilon = \frac{\|\mathrm{E_{rec}} - \mathrm{E_{ref}}\|_2}{\|\mathrm{E_{ref}}\|_2} \tag{4}$$

Where:

$E_{\mathrm{rec}}$: denotes the reconstructed electric field obtained using the SRM algorithm

$E_{\mathrm{ref}}$ : represents the corresponding theoretical or simulated reference field sampled over the same angular grid.

This measure offers a normalized estimate of the difference between the reconstructed field and the reference field. This measure is commonly used for the solution of various problems related to the inversion of electromagnetic fields as well as source reconstruction problems. The error evaluation procedure, as an illustrative example, involves the evaluation of the Euclidean norm of the difference between the reconstructed field and the reference field, $\| E_{\mathrm{rec}} - E_{\mathrm{ref}} \|_2$, as well as the normalization of the obtained result by the energy of the reference field, $\| E_{\mathrm{ref}} \|_2$. For instance, at a signal-to-noise ratio of 20 dB, the procedure provided a relative error estimate of $\varepsilon \approx 0.09$, which indicates that the reconstructed field deviates from the theoretical pattern by less than 10%.

 

For example, when the SNR is set to 20 dB, the relative error in reconstruction was determined by comparing the reconstructed far-field patterns using SRM and the theoretically computed far-field patterns over the entire range of angles of interest, yielding a normalized error of approximately $\varepsilon \approx 0.09$. To validate the robustness of this approach in the presence of measurement noise, AWGN was added to the AOA-only far-field data under various SNR environments. The SRM approach was applied when the SNR was set to 10 dB, 20 dB, and 30 dB. The errors obtained are presented in Table 1. The results clearly demonstrate that the proposed system achieves stable performance for reconstruction with moderate noise conditions, where the relative error monotonically decreases with increasing SNR. At an SNR of 20 dB, which is typical for antenna measurement conditions, the error for reconstruction is always below 10%, validating the robustness of the proposed regularized amplitude-only SRM approach.

**Table 1:** Reconstruction error versus SNR

| Item No | SNR(dB) | Relative Error ($\varepsilon$) |
|---|---|---|
| 1 | 10 | ~0.18 |
| 2 | 20 | ~0.09 |
| 3 | 30 | ~0.04 |

The convergence of this iterative process was also verified by monitoring the variation of the reconstruction error during this process. In this study, during the numerical tests performed, it was observed that the reconstruction error was decreasing during this iterative process, reaching a constant value after a certain number of iterations. After this point, it was observed that during further iterations, no changes in the reconstructed fields were observed, thereby verifying that the proposed framework is numerically convergent for this scenario of SRM. This evaluation verifies that not only is the proposed framework in agreement with theoretical predictions, but it is also numerically stable, consistent, and robust under practical noise scenarios.

## 5. CONCLUSION

This work proposes a MATLAB-based tool for antenna diagnostics, which combines the use of only the amplitude of the field measurements with the Source Reconstruction Method (SRM) in a completely interactive GUI. The developed tool can accommodate any type of antenna, any type of array, 2D radiation pattern visualization, Direction of Arrival (DoA) detection, null detection, as well as the estimation of the excitation current from the measurements. The results obtained with the developed tool can accurately reconstruct the current distribution, making the tool a cost-effective solution for antenna diagnostics, not only for research purposes but also for modern wireless communication systems. The developed tool can be enhanced to include error analysis, making the tool more efficient for the solution of the problems related to the use of the SRM, which can transform the current resource-intensive process into a more efficient solution for the characterization of antennas without the use of intricate phase measurements. With its robustness, accuracy, and ease of use, the tool is expected to make a significant contribution to the current research in the field of antennas. In conclusion, the SRM tool based on the MATLAB platform offers a useful and cost-effective method for the non-invasive diagnosis of antennas based on amplitude-only measurements. The tool has the potential to progress to a reliable tool for the testing of antennas, phased arrays, and satellite antennas.

## REFERENCES

[1] Greengard L, Rokhlin V. A Fast Algorithm for Particle Simulations. Journal of Computational Physics. 1997;135(2):280-92. doi:10.1006/jcph.1997.5706

[2] Las-Heras F, Sarkar TK. A direct optimization approach for source reconstruction and NF-FF transformation using amplitude-only data. IEEE Transactions on Antennas and Propagation. 2002;50(4):500-10. doi:10.1109/tap.2002.1003386

[3] Álvarez Y, Las-Heras F, Pino MR. The sources reconstruction method for amplitude-only field measurements. 2010 IEEE Antennas and Propagation Society International Symposium; 2010/07: IEEE; 2010. p. 1-4. doi:10.1109/aps.2010.5562290

[4] Cappellin C, Pivnenko S. Application aspects of advanced antenna diagnostics with the 3D reconstruction algorithm. 2015 European Radar Conference (EuRAD); 2015/09: IEEE; 2015. p. 293-6. doi:10.1109/eurad.2015.7346295

[5] Chen C, Hong J, Ji L. Intrinsic Properties of Stochastic Maxwell Equations. Lecture Notes in Mathematics: Springer Nature Singapore; 2023. p. 63-95. doi:10.1007/978-981-99-6686-8_3

 

[6] Peterson AF, Ray SL, Mittra R, editors. Computational Methods for Electromagnetics: IEEE; 1997. doi:10.1109/9780470544303

[7] Álvarez López Y, García Fernández M, Laviada Martínez J, Las-Heras Andrés F. Improving the Performance of the Phaseless Sources Reconstruction Method for Antenna Diagnostics and Characterization. IEEE Open Journal of Antennas and Propagation. 2025;6(3):915-27. doi:10.1109/ojap.2024.3393432

[8] Borden B. Mathematical problems in radar inverse scattering. Inverse Problems. 2001;18(1):R1-R28. doi:10.1088/0266-5611/18/1/201

[9] Bevilacqua F, Capozzoli A, Curcio C, D'Agostino F, Ferrara F, Gennarelli C, et al. A Phaseless Near-Field to Far-Field Transformation With Planar Wide-Mesh Scanning Accounting for Planar Probe Positioning Errors. IEEE Access. 2023;11:132735-49. doi:10.1109/access.2023.3330629

[10] Li P, Jiang L. An Iterative Source Reconstruction Method Exploiting Phaseless Electric Field Data. Progress In Electromagnetics Research. 2013;134:419-35. doi:10.2528/pier12102105

[11] Cano-Facila FJ, Burgos S, Martin F, Sierra-Castaner M. New Reflection Suppression Method in Antenna Measurement Systems Based on Diagnostic Techniques. IEEE Transactions on Antennas and Propagation. 2011;59(3):941-9. doi:10.1109/tap.2010.2103035

[12] Rahmat-Samii Y. Electromagnetic Band Gap Structures: Advances in Computational Techniques. Integrated Photonics Research: OSA; 1999. p. RTuE4. doi:10.1364/ipr.1999.rtue4

[13] Hansen RC. Phased Array Antennas: Wiley; 2009 2009/11/16. doi:10.1002/9780470529188

[14] Volakis JL, Sertel K. Integral Equation Methods for Electromagnetics. Institution of Engineering and Technology; 2012. doi:10.1049/sbew045e

[15] Song JM, Chew WC. Multilevel fast-multipole algorithm for solving combined field integral equations of electromagnetic scattering. Microwave and Optical Technology Letters. 1995;10(1):14-9. doi:10.1002/mop.4650100107

[16] Fuchs B, Coq LL, Migliore MD. Fast Antenna Array Diagnosis from a Small Number of Far-Field Measurements. IEEE Transactions on Antennas and Propagation. 2016;64(6):2227-35. doi:10.1109/tap.2016.2547023

[17] Razavi SA, Neshati MH. Development of a Low-Profile Circularly Polarized Cavity-Backed Antenna Using HMSIW Technique. IEEE Transactions on Antennas and Propagation. 2013;61(3):1041-7. doi:10.1109/tap.2012.2227104

[18] Scherzer O. A parameter choice for Tikhonov regularization for solving nonlinear inverse problems leading to optimal convergence rates. Applications of Mathematics. 1993;38(6):479-87. doi:10.21136/am.1993.104570

[19] Porfirev AP. Modification of the Gerchberg-Saxton algorithm for the generation of specle-reduced intensity distributions of micrometer and submicrometer dimensions. Optik. 2019;195:163163. doi:10.1016/j.ijleo.2019.163163

[20] Harrington RF, editor. Field Computation by Moment Methods: IEEE; 1993. doi:10.1109/9780470544631

[21] Appel-Hansen J. Near-Field Far-Field Antenna Measurements. Antenna Handbook: Springer US; 1988. p. 2175-205. doi:10.1007/978-1-4615-6459-1_33

[22] Brown T, Jeffrey I, Mojabi P. Multiplicatively Regularized Source Reconstruction Method for Phaseless Planar Near-Field Antenna Measurements. IEEE Transactions on Antennas and Propagation. 2017;65(4):2020-31. doi:10.1109/tap.2017.2670518

[23] Bod M, Moradi G, Sarraf-shirazi R. Phaseless near-field to far-field transformation based on source current reconstruction and signal subspace optimization. International Journal of RF and Microwave Computer-Aided Engineering. 2021;32(1). doi:10.1002/mmce.22913

[24] Wei JG, Peng Z, Lee JF. Multiscale electromagnetic computations using a hierarchical multilevel fast multipole algorithm. Radio Science. 2014;49(11):1022-40. doi:10.1002/2013rs005250

 